This is an Accepted Manuscript for *Journal of Glaciology*. Subject to change during the editing and production process.
DOI: 10.1017/jog.2024.25

Ice volume and thickness of all Scandinavian glaciers and ice caps

Thomas FRANK,[1] Ward VAN PELT,[1]

[1] *Department of Earth Sciences, Uppsala University, Uppsala, Sweden*

Correspondence: Thomas Frank <thomas.frank@geo.uu.se>

ABSTRACT. We present a new map of bed topography and ice thickness together with a corresponding ice volume estimate representative of the years around 2010 for all Scandinavian ice caps and glaciers. Starting from surface observations, we invert for ice thickness by iteratively running an innovative ice dynamics model on a distributed grid and updating bed topography until modelled and observed glacier dynamics as represented by their rate of surface elevation change (dh/dt) fields align. The ice flow model used is the Instructed Glacier Model (Jouvet and Cordonnier, 2023), a generic physics-informed deep-learning emulator that models higher-order ice flow with high computational efficiency. We calibrate the modelled thicknesses against >11,000 ice thickness observations, resulting in a final ice volume estimate of 302.7 km^3 for Norway, 18.4 km^3 for Sweden and 321.1 km^3 for the whole of Scandinavia with an error estimate of about $\pm 11\%$. The validation statistics computed indicate good agreement between modelled and observed thicknesses (RMSE = 55 m, Pearson´s r = 0.87, bias = 0.8 m), outperforming all other ice thickness maps available for the region. The modelled bed shapes thus provide unprecedented detail in the subglacial topography, especially for ice caps where we produce the first maps that show ice-dynamically realistic flow features.

1 INTRODUCTION

As a result of global climate warming, glaciers and ice caps are projected to shrink and retreat in all regions on Earth, continuing on the current trajectory of large-scale ice loss (Oppenheimer and others, 2019; Rounce and others, 2023). Any assessment of ensuing consequences is dependent on knowledge of the ice volume existing today. This concerns not only projections of sea-level rise, but also water management in general where the regional ice volume can be a key determinant for the future availability of water for basic needs and irrigation (e.g. in the Himalayas (Pritchard, 2019)), or for hydro-power production, as in Scandinavia (Ekblom Johansson and others, 2022). Besides total ice volume, knowledge of the spatial distribution of ice within a region, between different glaciers and within one glacier is crucial. Such maps of ice thickness and, thereby, subglacial topography are essential for future projections of glacier response to climate warming as the bed shape controls the future hypsometric distribution of ice, and through that, whether a glacier will be able to stabilize at higher elevations (Rounce and others, 2023). For marine terminating glaciers, subglacial topography is crucial in determining the dynamical response to an external signal, and consequently, whether stabilization (e.g. on pinning points or bathymetric highs) or retreat of the grounding line (e.g. due to inland sloping beds) is likely to occur (Åkesson and others, 2018; Frank and others, 2022). The location of future lakes and the routing of future rivers can likewise be deduced from the shape of the glacier bed (Farinotti and others, 2019b; Ekblom Johansson and others, 2022). Furthermore, ice thickness maps can help both the tourism industry and scientists on fieldwork to plan economic or scientific investments (Marr and others, 2022). Importantly, knowledge of subglacial topography also helps to assess the risks associated with future deglaciated landscapes, e.g. the potential for glacier lake outburst floods or landslides (Liestøl, 1956; Engeset and others, 2005; Breien and others, 2008; Jackson and Ragulina, 2014). Finally, the topography of future exposed lands is important in shaping the emerging habitats that form when glaciers retreat (Bosson and others, 2023).

To estimate ice volume and bed shape while overcoming the lack of ice thickness observations for most glaciers in the world (GlaThiDa Consortium, 2020; Welty and others, 2020) inversion techniques have been developed that allow the derivation of subglacial topography based of surface observations. The recent years have seen continued progress in this field (Farinotti and others, 2017, 2021), expanding from early works on volume-area scaling (Bahr and others, 1997, 2014) to techniques such as shear-stress based approaches (e.g. Nye, 1952; Linsbauer and others, 2009; Frey and others, 2014) and mass-conservation approaches (e.g.

https://doi.org/10.1017/jog.2024.25 Published online by Cambridge University Press

Farinotti and others, 2009; Huss and Farinotti, 2012). With the advent of high-quality remote sensing products regional-scale ice flow velocity-based approaches have become possible (e.g Gantayat and others, 2014; Millan and others, 2022) alongside methods involving full ice dynamics models on distributed grids that require a combination of several observational data sets (e.g. ice velocity fields, dh/dt) and/or auxiliary model products (e.g. from a mass balance model) as inputs (van Pelt and others, 2013; Jouvet, 2022; Frank and others, 2023).

While some ice volume estimates for Scandinavia have been proposed in the early 2010s (Radić and Hock, 2010; Marzeion and others, 2012; Huss and Farinotti, 2012; Grinsted, 2013; Andreassen and others, 2015), the methodological limitations associated with these approaches have prevented the creation of distributed maps of ice thickness. Such products only became available recently when Farinotti and others (2019a) and Millan and others (2022) mapped ice thickness on a global scale. However, the large-scale perspective of these works, the methodological limitations of each approach (sec. 6), the large uncertainties reported for Scandinavia ($> \pm 25\%$ of total calculated ice volume in both studies) and the fact that the two approaches have led to wildly different outcomes in some areas on the globe leave the question whether their results are reliable for Scandinavia. Therefore, we here produce a new ice volume estimate, and ice thickness and bed topography maps for all glaciers and ice caps in Scandinavia. We follow a recent methodology developed in Frank and others (2023) which showed excellent performance in a variety of settings. A novelty in the approach is the use of the machine learning based Instructed Glacier Model (IGM; Jouvet and Cordonnier, 2023) which allows us to employ higher-order ice physics on a regional scale.

2 STUDY AREA

According to the Randolph Glacier Inventory v6.0 (RGI Consortium, 2017), hereafter referred to as RGI60, based on mapping from Andreassen and others (2012), Scandinavia hosts 3,417 glaciers covering a total area of 2,949 km^2 (Fig. 1). The median and mean glacier size is 0.2 km^2 and 0.9 km^2, respectively. 3,130 of these glaciers are located in Norway, 283 in Sweden, and 4 in the Fennoscandian part of Russia which were included as nominal glaciers in the RGI60, yet their their outlines are missing and so they are not considered here. Note that there is a recent update of glacier outlines for Norway by Andreassen and others (2022) which, however, we do not use due to practical issues related to their compatibility with other input products (see sec. 4 for more details).

https://doi.org/10.1017/jog.2024.25 Published online by Cambridge University Press

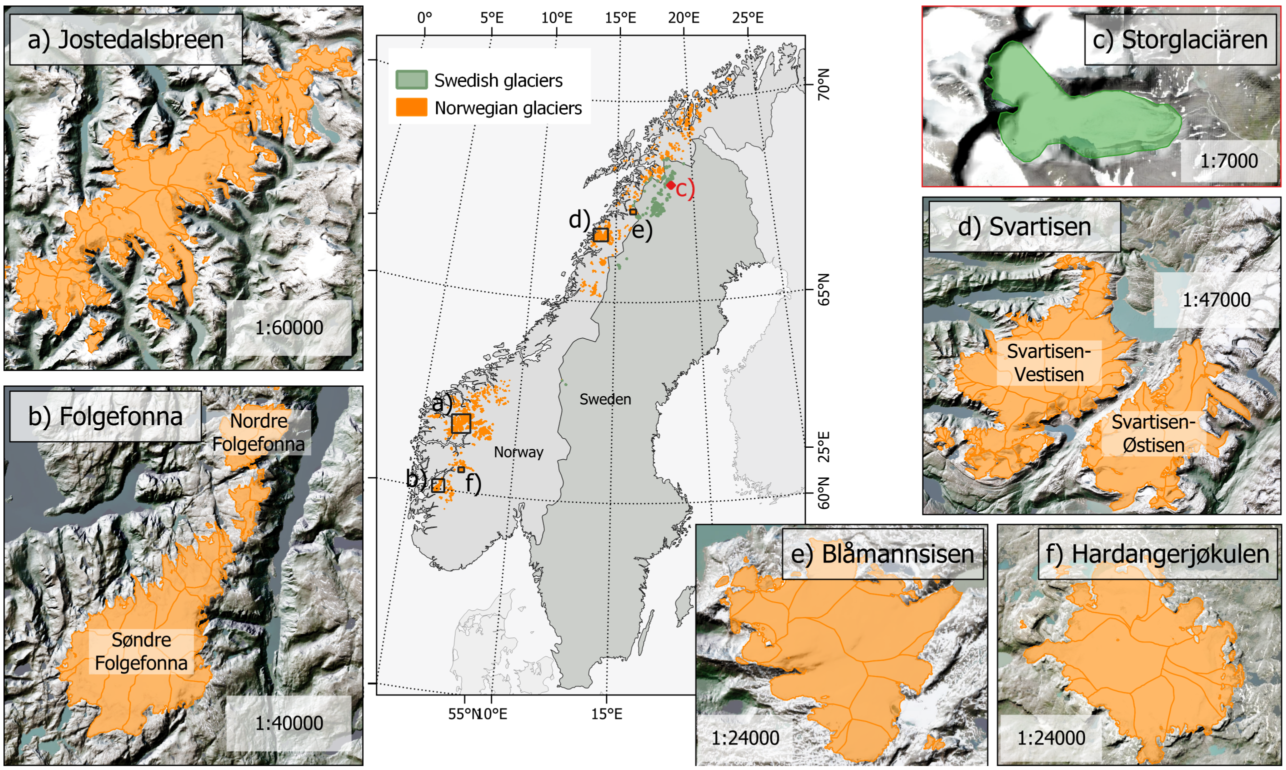

Fig. 1. Geographical distribution of glaciers in Sweden and Norway with zoom to Jostedalsbreen (a), Folgefonna with its Northern part Nordre Folgefonna and Southern part Søndre Folgefonna (b), Storglaciären (c), Svartisen with its Western ice cap Svartisen-Vestisen and Eastern ice cap Svartisen-Østisen (d), Blåmannsisen (e) and Hardangerjøkulen (f). Glacier outlines are taken from the RGI60 (RGI Consortium, 2017), orginally compiled by Andreassen and others (2012) for Norway. Note that in the context of this study, adjacent RGI60 glaciers are merged together in *glacier complexes* to avoid introducing artificial steps in bed topography between them (sec. 4). Background imagery includes ArcGis World Imagery ©Esri.

https://doi.org/10.1017/jog.2024.25 Published online by Cambridge University Press

After Scandinavia was completely covered by the Fennoscandian ice sheet during the last glacial maximum, the ensuing deglaciation resulted in ice-free conditions by the early Holocene (Stroeven and others, 2016). The glaciers of today are thought to have re-emerged and grown after the mid-Holocene, interrupted by smaller retreat phases (Karlén, 1973; Karlén and Matthews, 1992). After having reached the most recent maximum extent around the mid 17-hundreds in the context of the Little Ice Age (Grove, 2004), the past century has been characterized by glacier retreat, although periods with positive mass balances have been recorded after the 1960s as well (Holmlund and others, 1996; Andreassen and others, 2020). Today, mass loss clearly dominates and future projections for Scandinavia suggest close to ice-free conditions with 93±9% mass loss relative to 2015 by the end of the century under the RCP8.5 scenario. Even under the more optimistic RCP2.6 scenario wide-spread deglaciation is projected, as shown by an estimated mass loss of 72±33% (Rounce and others, 2023).

Due to Sweden´s location on the leeward side of the Scandes the climate there is considerably drier than on the maritime Norwegian side to the West. Accordingly, the predominant glacier types are mountain and cirque glaciers of smaller size, and their geographical distribution is concentrated in the North of the country, namely in the Sarek area and the mountains of the Kebnekaise massif (Fig. 1). There is no ice cap in Sweden. Of Sweden´s glaciers, Storglaciären is best known and has been the subject of numerous studies (Fig. 1c; e.g Pohjola, 1993; Hooke and others, 1989; Holmlund and Eriksson, 1989; Fountain and others, 2005; Hock and Holmgren, 2005; Terleth and others, 2023). Storglaciären is also the site of the longest mass balance observation time series in the world using the direct glaciological method (Holmlund and Jansson, 1999). Despite this long tradition of glaciological studies, there are only a few thickness observations publicly available for Sweden (Björnsson, 1981) with the global Glacier Thickness Database (GlaThiDa) listing no entry for the country (GlaThiDa Consortium, 2020; Welty and others, 2020).

Norwegian glaciers generally have steeper mass balance gradients and accordingly higher mass fluxes owing to their maritime setting. High precipitation has allowed the formation of six ice caps (Jostedalsbreen, Svartisen-Vestisen, Svartisen-Østisen, Folgefonna, Blåmannsisen and Hardangerjøkulen; Fig. 1a,b,d,e,f) characterized by low surface slopes at the top and outlet glaciers extending into surrounding valleys. The glacier cover, totalling 2669 km^2 according to the RGI60 and 2328±70 km^2 according to Andreassen and others (2022), is somewhat more extensive in the South of the country (57% or 60% of glacier area following those references) compared to the North (43% / 40%) (Andreassen and others, 2012, 2022). Numerous thickness observations have been collected throughout the past decades which were compiled by Andreassen

https://doi.org/10.1017/jog.2024.25 Published online by Cambridge University Press

and others (2015).

3 METHODS

3.1 Inversion methodology

The inversion methodology is based on Frank and others (2023), and inspired by van Pelt and others (2013). It was applied in different settings and showed excellent performance for benchmark glaciers of the Ice Thickness Modelling Intercomparison eXperiment (ITMIX; Farinotti and others, 2017, 2021). The method relies on iteratively updating an initial guess of bed topography inside a domain defined by observed glacier outlines. Specifically, in each iteration, a new bed B^{i+1} is produced based on the mismatch between observed and modelled rates of surface elevation change dh/dt such that

$$B^{i+1} = B^i - \beta \left(\frac{dh^i_{\mathrm{mod}}}{dt} - \frac{dh_{\mathrm{obs}}}{dt} \right) \tag{1}$$

where B^i is the bed elevation from the previous iteration and β is a scalar controlling the strength of bed updates applied in each iteration i. To obtain dh/dt_{mod}, an ice flow model forced with a prescribed climatic mass balance $\dot{b}$ is run forward over a short time span dt (Frank and others, 2023). The rationale behind eq. (1) is to find the bed which is consistent with the dynamic state of a given glacier as represented by its dh/dt_{obs} field, implying that no steady-state assumption is made. Instead of applying eq. (1) directly, however, one may also use available dh/dt observations and a climatic mass balance product to compute the apparent mass balance $\tilde{b}$ (Farinotti and others, 2009), and feed that to the forward model instead of $\dot{b}$. $\tilde{b}$ represents the climatic mass balance that would be needed for the glacier in its present shape to be in steady-state. We do that here due to benefits in producing consistent input data (sec. 4) which, considering that dh/dt_{obs} is thus already incorporated in the mass balance that the forward model sees, requires us to set $dh/dt_{\mathrm{obs}} = 0$ in eq. (1) when applying the bed updates.

To avoid introducing small-scale features in the bed solution not justified by the input data and to prevent fitting to errors regularization is needed (Habermann and others, 2012). As detailed in Frank and others (2023), this is done by adjusting the surface as a small fraction θ of the bed updates but in the opposite direction such that a new surface S^{i+1} is given by

$$S^{i+1} = S^i + \theta\beta \left(\frac{dh^i_{\mathrm{mod}}}{dt} - \frac{dh_{\mathrm{obs}}}{dt} \right). \tag{2}$$

https://doi.org/10.1017/jog.2024.25 Published online by Cambridge University Press

The surface updates locally change the driving stress (e.g. where the bed becomes deeper, the surface height increases, and thus the surface gradient and ice flow to surrounding grid cells is enhanced) resulting in a regular distribution of ice, while allowing the model to accommodate errors in the input data through small surface changes rather than large bed adjustments (Gudmundsson, 2003). As shown in Frank and others (2023), a larger value for θ leads to a smoother thickness field but it also increases the dependence on the initial bed because more of the dh/dt misfit is accommodated by surface updates rather than bed changes.

3.2 Ice flow model

The ice flow model used is the physics-informed deep learning based Instructed Glacier Model v2.0.4 (IGM; Jouvet and Cordonnier (2023)) which builds on, yet significantly improves an earlier version (Jouvet and others, 2022; Jouvet, 2022). IGM represents a fusion between classical finite element and deep learning methods in that the mass continuity equation

$$\frac{dh}{dt} + \nabla \cdot (\bar{\mathbf{u}} h) = \dot{b} \tag{3}$$

is solved where the ice flow velocities $\bar{\mathbf{u}}$ are obtained from a Convolutional Neural Network (CNN). However, IGM not only relies on the CNN but also on a higher-order solver which is used to re-train the CNN in regular intervals during transient model runs.

Specifically, the ice viscosity dependent higher-order ice flow approximation (Blatter, 1995; Pattyn, 2003) including a Weertman-type sliding law (Weertman, 1957) is formulated as a minimization problem where a loss function seeks to find the ice velocity that minimizes the energy associated with the higher-order equations on a regular 2D grid (eq.(18) in Jouvet and Cordonnier (2023)). While the solver finds the ice velocities by actually solving the minimization equation, the CNN seeks to obtain the same result, although through optimizing its weights. As such, the CNN learns the actual higher-order ice flow equation which as a result can be regarded as being encoded in the structure and weights of the CNN. This strategy is superior to the earlier versions of IGM that merely 'copied' the solutions obtained from a full-Stokes instructor model (Jouvet and others, 2022) as it makes the CNN independent of an instructor model and the limited training data simulated with it. To ensure a close agreement between the emulator and solver solutions in transient simulations the CNN is retrained at a user-defined interval (here chosen to be the default setting of every 5th model iteration). This means that at those instances, the solver is run to

https://doi.org/10.1017/jog.2024.25 Published online by Cambridge University Press

calculate the minimal energy associated with the current model state, followed by an update of the CNN weights such that the solution of the emulator is as close as possible to that of the solver. Due to the re-training strategy and the fact that the equation itself is learned, IGM can in principle be used with any spatial resolution and for any glacier type (as demonstrated by the application to an ice shelf in Jouvet and Cordonnier (2023)), in contrast to the previous IGM versions which were limited to a few possible resolutions and applications that were within the 'hull' defined by the training data (Jouvet and others, 2022; Jouvet, 2022). Thanks to the low computational cost of evaluating the CNN and because IGM is coded in a highly parallelized manner favorable for running on graphics processing units (GPU), IGM is efficient and allows us to use more advanced ice flow physics than previous studies on a regional scale.

3.3 Inversion workflow and parameter choices

To obtain an initial guess for ice thickness and bed topography, we use the perfect plasticity assumption (Nye, 1952) given by

$$h = \frac{\tau_b}{\rho g \sin\alpha}, \tag{4}$$

where h is ice thickness, $\rho = 910$ kg m^{-3} is the ice density, α is surface slope, $g = 9.8$ m s^{-2} is gravitational acceleration and τ_b is the basal shear stress. We estimate τ_b based on Haeberli and Hoelzle (1995) who established a parameterization relating glacier hypsometry to average basal shear stress along the central flowline of glaciers in the Alps. Note that while this may be a crude approach, especially for ice caps, we do not see a significant impact of the initial ice thickness on the final result. Then, using the ice flow model IGM set up with observations of surface height, an apparent mass balance field, a glacier mask, the initial guess of bed topography and a calibrated estimate on ice viscosity and sliding coefficient (sec. 3.4, 4), we simulate 5000 model years in which we update bed and surface based on eq. (1) and (2). The regularization parameter θ is 0.05 as in Frank and others (2023).

To stabilize the inversion and aid convergence, we let β increase with each iteration i as in Frank and others (2023) such that

$$\beta = \frac{-i_s \cdot \beta_0}{i + i_s} + \beta_0 \tag{5}$$

where β_0 is 1 and i_s is 20.

This workflow, in general, allows to obtain a spatially distributed ice thickness map. However, due to

https://doi.org/10.1017/jog.2024.25 Published online by Cambridge University Press

imperfections in the representation of reality by the model and due to data errors, some ice may be leaving the glacier outlines laterally or at the front in each iteration, in which case other areas inside the domain remain ice-free. The magnitude of this 'mass leakage rate' can be calculated as the integrated climatic mass balance of the ice-free areas since that is the amount of mass missing to close the mass budget of a glacier inside its domain. To enable a closure of the mass budget, we add the total mass leakage rate divided by the glacier area to the specific apparent mass balance at each grid cell in the domain 2000 model years before the end of the simulation when the glacier already has reached a steady state. The ensuing advance of the glacier brings the mass budget closer to zero, although we note that in some cases, some of the added mass may be leaking out laterally or at the front too, meaning that areas within the glacier outline remain ice-free. While another round of mass balance updates could resolve this, the fact that we do not know where exactly the leaking ice would have flown if the model and reality were perfectly aligned means that distributing the mass addition spatially uniformly carries the danger of much too-thick ice in some parts of the domain. Hence, we stick with one mass balance update and instead fill holes in the ice thickness (i.e. where the ice thickness is smaller than 15 m; corresponding to on average ∼8% of glacier area in this study) at the end of the inversion process through linear interpolation. In a final step, we apply a two-sigma Gaussian filter to the solution while taking into account local ice thickness and whether or not a given grid cell was interpolated. Specifically, we normalize the ice thickness field relative to a maximum value of 500 m. In the resulting norm raster (with values between 0 and 1), interpolated grid cells are also assigned 1, regardless of their thickness. The final ice thickness at each grid cell is then calculated as the sum of the smoothed ice thickness multiplied by the norm raster plus the non-smoothed thickness multiplied by 1 minus the norm raster. This approach allows to preserve small details in the bed shape where the ice is thin, while it removes such details where the ice is thick following the principle that there is an inverse relationship between the detail that can be possibly obtained through an inversion and ice thickness (Gudmundsson, 2003; Raymond and Gudmundsson, 2005)

3.4 Calibration, validation and error estimation using thickness observations

Calibration

We calibrate our model results against all ice thickness observations (h_{obs}) available for Scandinavia in the Glacier Thickness Database (GlaThiDa Consortium, 2020; Welty and others, 2020) and a bed elevation model of Storglaciären (Björnsson, 1981) ($\text{n}_{\text{obs\_total}} > 11,000$). This is done by tuning the region-wide

https://doi.org/10.1017/jog.2024.25 Published online by Cambridge University Press

rate factor A and the friction coefficient c of the Weertman sliding law (eq. 10 in Jouvet and Cordonnier (2023)). However, we exclude the observations of Jostedalsbreen from the region-wide calibration since we find that the errors in the modelled thicknesses are significantly larger than those at all other glaciers, indicating that Jostedalsbreen is not representative of the remaining glaciers (sec. 5). Jostedalsbreen is calibrated separately based on its observations. The remaining observations cover 10 glacier complexes (c.f. sec. 4) of different size, type and geographical distribution. Note that whether or not to correct the thickness observations for surface elevation changes that may have occurred since radar data acquisition has no appreciable effects on the results. This is in line with the general absence of trends in the mass balance of Scandinavian glaciers from the 1950s up until the 2000s (Holmlund and others, 1996; Andreassen and others, 2020). In this study, all mentions of thickness observations refer to the actual thickness values reported in the GlaThiDa. To allow constraining the two unknowns A and c against only one set of observations, we follow a similar approach as in Jouvet (2022) and assume that A cannot be larger than 78 MPa^{-3}a^{-1} (corresponding to the typical value used for temperate ice (Cuffey and Paterson, 2010)) while sliding beyond a set minimum given by $c = 100$ km MPa^{-3}a^{-1} cannot occur for cold ice, i.e. when $A < 78$ MPa^{-3}a^{-1}. Although this approach is a simplification that does not reflect the complex polythermal nature of glaciers in Scandinavia (Pettersson and others, 2003) as well as their possibly enhanced viscous deformation due to high liquid water content resulting from their maritime setting, it is chosen here since it allows to place A and c on one continuous scale with a unique solution for the combination of the two that minimizes the misfit to observations, and hence ensures an unbiased total ice volume estimate with respect to the observations.

To obtain the optimized A and c, we consider two different strategies: 1) Minimizing the mean difference between modelled and observed thickness on a point-by-point basis for all observations pooled together; 2) For each glacier complex, determine the values for A and c which minimize the point-by-point bias for that glacier, and then select the A, c combination corresponding to the mean or median of the ranks of the sorted A, c combinations tested (note that for creating an evenly spaced A, c scale necessary for calculating means and medians of the A, c ranks, we find that setting a 5 MPa^{-3}a^{-1} change in A equal to a 500 km MPa^{-3}a^{-1} change in c is appropriate). While the former approach assigns equal weights to each thickness observation, the latter instead assigns equal weight to each glacier with observations. We find that following strategy 1 as well as taking the mean of the A, c ranks of strategy 2 yields the same optimal combination $A = 70$ MPa^{-3}a^{-1}, $c = 100$ km MPa^{-3}a^{-1}, whereas the median of strategy 2 gives

https://doi.org/10.1017/jog.2024.25 Published online by Cambridge University Press

$A = 78$ MPa^{-3}a^{-1}, $c = 100$ km MPa^{-3}a^{-1}. Given that two of the three indicators favor the former and since that A, c combination also yields overall better validation statistics, we settle for $A = 70$ MPa^{-3}a^{-1} and $c = 100$ km MPa^{-3}a^{-1}. The obtained values are close to what one would expect for Scandinavian glaciers ($A = 70$ MPa^{-3}a^{-1} corresponds to an ice temperature of ~ -0.6°C) which are generally thought to be temperate but often feature cold surface layers (Pettersson and others, 2003; Andreassen and others, 2012), suggesting that there are no major biases in our setup which need to be compensated by the calibration process. For Jostedalsbreen where we test a large parameter space of A and c to obtain the best validation statistics, we find an optimal combination $A = 70$ MPa^{-3}a^{-1}, $c = 1000$ km MPa^{-3}a^{-1}, i.e. elevated sliding is required to match the thickness observations best. Whether or not this represents a physical process is unclear given that the calibration of A and c against observations implies that all errors in the study setup (including those in the observations) are subsumed in these parameters.

Validation

The results are validated against the same set of thickness observations. Using the same set of observations for calibration and validation is not considered problematic here given that only Scandinavia-wide parameters are tuned against observations, while the validation is done on a point-by-point basis. We consider the RMSE and the mean absolute difference (MAD), both indicative of how far (in absolute terms) the modelled ice thickness is off from the observed one at any given point on a glacier; the mean difference/bias, showing whether the average ice thickness and thus total ice volume is over- or underestimated; and Pearson´s correlation coefficient r between modelled and observed thicknesses which, too, indicates how well modelled and observed bed shapes agree. In addition, we calculate the slope of the linear regression between $\mathrm{h_{mod}}$ and $\mathrm{h_{obs}}$ to evaluate whether both high and low thicknesses are matched as well as the relative difference in variance $\Delta\sigma^2 = \left(\sigma^2_{\mathrm{mod}} - \sigma^2_{\mathrm{obs}}\right)/\sigma^2_{\mathrm{mod}}$ of ice thickness values at those locations where observations exist. The latter is a measure for how smooth the modelled bed shapes are in relation to the observations.

Furthermore, a direct volume validation is performed against five glacier complexes (Nordre Folgefonna, Søndre Folgefonna, Hardangerjøkulen, Blåmannsisen and Storglaciären) which have such dense radar coverage that their true volume can be assumed to be known (Björnsson, 1981; Andreassen and others, 2015; Ekblom Johansson and others, 2022).

https://doi.org/10.1017/jog.2024.25 Published online by Cambridge University Press

Error estimation

Since we calibrate the rate factor A and the sliding coefficient c, and through that the total ice volume, against observed thicknesses, an error estimation on the total ice volume can be made by varying A and c. If we had ice thickness observations that could be assumed entirely representative of the "true" ice thickness distribution, tuning A and c so that the mean misfit with observations is zero would give an accurate Scandinavia-wide ice volume. However, since we do not know whether the thickness observations are representative, we ask the following question: If the sample of thickness observations was biased towards glaciers which are well-represented with high (low) values for A and c, what are plausible lowest (highest) values for the A, c combination? To resolve this question, we consider the results from strategy 2 above, and remove the highest and lowest A, c combination obtained for the 10 glacier complexes. Based on that, we are left with a range $(A, c) \in \{(50, 100), (78, 1500)\}$ which covers 8 out of 10 glacier complexes, and thus can be assumed plausible. With that, the results of the thickness inversion using $A = 50$ MPa^{-3}a^{-1} and $c = 100$ km MPa^{-3}a^{-1} form the high-end estimate for Scandinavian ice volume, while the values obtained using $A = 78$ MPa^{-3}a^{-1} and $c = 1500$ km MPa^{-3}a^{-1} mark the lower bound. To estimate the ice volume uncertainty of Jostedalsbreen, we assume the same range in A as for all other glaciers, but set c to 1000 km MPa^{-3}a^{-1} and 2500 km MPa^{-3}a^{-1} in the upper and lower ice volume scenarios, respectively, following the results from the calibration where it was found that this glacier complex generally requires more sliding.

Further errors in the total ice volume could result from errors in the glacier outlines. Andreassen and others (2022) suggest that an area uncertainty of up to 3% can be expected. If the outlines are too small, we do not know the ice thickness of the excluded areas. If the outlines are too big, it is likewise not possible to directly estimate how this would have affected the glacier thickness distribution inside these outlines, and thereby the ice volume overestimation of our result. Therefore, we simply assume that the volume uncertainty from glacier outlines is $\pm 3\%$ of the total ice volume.

Deriving a formal error estimate on local ice thickness for each grid point in the domain is difficult since the main error source likely are ice flow errors (i.e. when the model directs ice in a different direction than where it flows in reality) which are hard to quantify. However, thanks to the available thickness observations, the mean absolute difference between h_{mod} and h_{obs} can serve as an indicator for expected errors.

https://doi.org/10.1017/jog.2024.25 Published online by Cambridge University Press

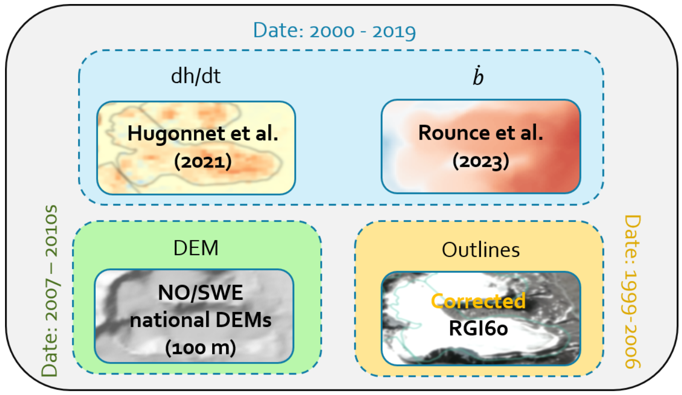

Fig. 2. Input data sets used in this study alongside their date of acquisition. dh/dt from Hugonnet and others (2021), climatic mass balance $\dot{b}$ from Rounce and others (2023), DEMs from the Norwegian and Swedish mapping authorities, outlines from the RGI60 (RGI Consortium, 2017) corrected for an obvious misalignment with the topography in Sweden.

4 INPUT DATA

As input to the inversion, we require a digital elevation model (DEM), spatially distributed climatic mass balance and dh/dt, as well as glacier outlines. Generally, we base our investigation on the RGI60 (RGI Consortium, 2017) and the glacier IDs therein which tie together the different input products. We, hence, do not use the updated outlines presented recently by Andreassen and others (2022) for Norway for the years 2018-2019 which have increased the number of glaciers by more than 2000 (covering an area of 48 km^2) while the total glacierized area in the country reduced by 15% due to glacier retreat (Andreassen and others, 2022). This is because the climatic mass balance and dh/dt input data sets described below are not available for these new outlines. Since the glaciers added in the newer inventory all are small (the largest is 0.205 km^2, and only 23 are larger than 0.1 km^2 (Andreassen and others, 2022)), ignoring them here is not expected to have a significant impact on the modelled ice volume. The glacier outlines in the RGI60 for Scandinavia were acquired between 1999 and 2006 with a mean year of acquisition in 2003. However, a systematic misalignment with the topography is evident for the Swedish glacier outlines, possibly as a result of reprojection errors that occurred when the outlines were transferred from their original source to the RGI60 database. We correct these issues by re-aligning the outlines with the topography which yields a substantial improvement as confirmed visually. The new outlines are submitted to the Global Land Ice Measurements from Space (GLIMS) database (Raup and others, 2007; Paul and others, 2016) and hence will be included in the next release of the Randolph Glacier Inventory. Note that the original shape of each

https://doi.org/10.1017/jog.2024.25 Published online by Cambridge University Press

outline is unaltered.

We use the national DEMs of Sweden and Norway in each country, respectively, with a 50 m resolution as provided by the national mapping authorities and stated elevation uncertainties of 5 m. The Norwegian DEM (Kartverket, 2013) is primarily from 2007, but has seen updates in different regions throughout the 2010s. The Swedish 50 m DEM (Lantmäteriet, 2022) is downsampled from the 1 m national DEM which was acquired between 2009 and 2019.

The dh/dt data are taken from Hugonnet and others (2021) who compiled rates of surface elevation change for all glaciers on Earth. Following Huss (2013), these volume changes are converted to mass changes assuming a density of 850 kg m^{-3}. The dh/dt data are available in 5-year bins from 2000 to 2019, but the signal in each bin alone may be contaminated considerably by noise. To avoid such issues we consider the entire 20-year period which yields the most stable signal.

The climatic mass balance $\dot{b}$ is taken from the global study by Rounce and others (2023) who modelled $\dot{b}$ in elevation bins for all glaciers on Earth for the 21st century. They performed an initial Bayesian calibration against the geodetic mass balance estimates from Hugonnet and others (2021) while validating against observations from the WGMS database (WGMS, 2022). For each glacier, we extract the years 2000-2019 to match the dh/dt data temporally and create a distributed field of climatic mass balance by applying the elevation-dependent $\dot{b}$ on the DEMs.

To close the mass budget of a glacier, it is necessary that

$$\int_\Omega \frac{dh}{dt} = \int_\Omega \dot{b} \tag{6}$$

where Ω is the glacier domain. Although Rounce and others (2023) calibrated their modelled $\dot{b}$ against dh/dt from Hugonnet and others (2021), the Bayesian approach does not guarantee that eq. (6) is fulfilled. Further issues arise from the fact that there are spatial inconsistencies between dh/dt and $\dot{b}$ in some places. For instance, dh/dt at the highest point in the accumulation area may be larger than $\dot{b}$, or comparably, dh/dt may be more negative than $\dot{b}$ in some places in the ablation area. Given that a glacier cannot gain more in ice thickness than what it receives in accumulation where there is no influx from above, and that the glacier cannot thin more than what it loses from melt in the ablation area unless there are large changes in the ice dynamics which are not known to have occurred in Scandinavia, both cases most likely represent data errors. To mitigate such issues, we apply the following workflow (Fig. 3): First, we calculate the

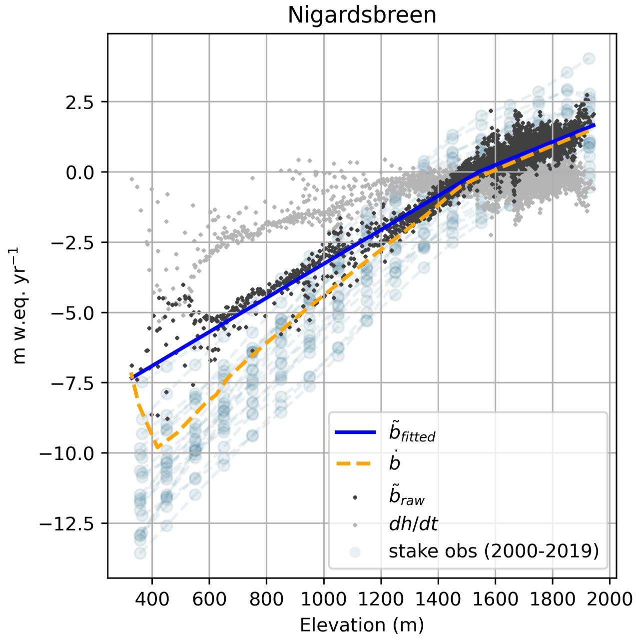

Fig. 3. Methodology for computing the apparent mass balance $\tilde{b}$ using the example of Nigardsbreen. Based on the stake observations of mass balance for the years 2000 - 2019 (where available) from WGMS (2022), Rounce and others (2023) derived the elevation dependent climatic mass balance $\dot{b}$. The difference between $\dot{b}$ and the spatially distributed dh/dt (taken from Hugonnet and others (2021)) is the apparent mass balance $\tilde{b}_{raw}$ (eq. (7)). $\tilde{b}_{raw}$ is then bias correct to obey eq. (6) (by 0.09 m w.eq. for Nigardsbreen; not shown as it would not be visible) before a piece-wise linear function with the nickpoint at the apparent ELA is fitted through $\tilde{b}_{raw}$ to obtain the final apparent mass balance $\tilde{b}_{fitted}$.

apparent mass balance (Farinotti and others, 2009) as

$$\tilde{b} = \dot{b} - \frac{dh}{dt}. \tag{7}$$

Next, we bias correct $\tilde{b}$ such that $\int_\Omega \tilde{b} = 0$. Finally, we fit an elevation-dependent piece-wise linear function with two segments through $\tilde{b}$ where we enforce the nickpoint at the apparent ELA. To ensure that $\tilde{b}$ is monotonically increasing with elevation, we do not allow negative slopes in any of the two segments of the piece-wise fit, and replace the piece-wise fit with a linear fit if that should be the case. As a result of these steps, applied to each glacier individually based on the climatic mass balance and dh/dt inputs, we obtain a smooth $\tilde{b}$ field that obeys eq. (6) and is physically consistent.

As a last step to input data preparation, we merge connected glaciers and all of their input fields together in one grid with 100 m resolution (Fig. 4). These *glacier complexes* are then modelled as one

https://doi.org/10.1017/jog.2024.25 Published online by Cambridge University Press

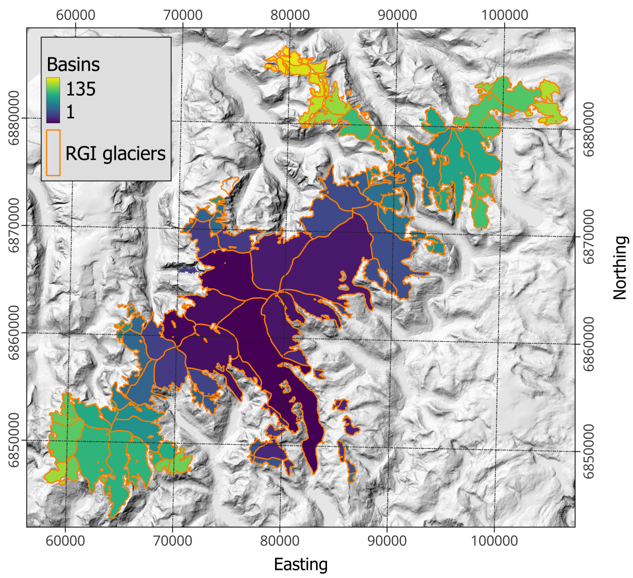

Fig. 4. The Jostedalsbreen ice cap as an example of a glacier complex (coordinate system is UTM 33N). All 135 RGI60 glaciers are modelled simultaneously on the same grid to not introduce inconsistencies at the boundaries between flow units. Note that the glacier complex shown here includes some glaciers that are formally not seen as part of Jostedalsbreen (Andreassen, 2022).

ice body which has the major advantage of preventing artificial boundaries and steps in modelled bed topography between connected glaciers. Particularly for ice caps where the RGI60 outlines may not always correctly delineate the actual flow units this is greatly advantageous as compared to modelling each RGI60 glacier individually.

5 RESULTS

5.1 Ice Volume

We find an ice volume of 302.7 km^3 for Norway and 18.4 km^3 for Sweden, summing to a total of 321.1 km^3 for all Scandinavian glaciers and ice caps. This corresponds to a sea level equivalent of 0.81 mm (based on eq. 7 in Millan and others (2022)). The mean glacier thickness is 113 m in Norway and 66 m in Sweden. The upper and lower bounds of ice volume estimated from varying A and c are 327.7/281.0 km^3 for Norway, 20.6/16.9 km^3 for Sweden and 348.3/297.9 km^3 in total. By adding the uncertainty on glacier outlines, the ice volume for Norway is between 272.5 and 337.5 km^3 ($h_{\text{mean\_NO}}$ in [102, 126] m), 16.4 and 21.2 km^3 for Sweden ($h_{\text{mean\_SWE}}$ in [59, 76] m), and 289.0 and 358.8 km^3 for entire Scandinavia. This corresponds to

https://doi.org/10.1017/jog.2024.25 Published online by Cambridge University Press

a total uncertainty of about ±11%. The six large ice caps Hardangerjøkulen, Jostedalsbreen, Folgefonna, Svartisen-Vestisen, Svartisen-Østisen and Blåmannsisen, all located in Norway and covering 1238.2 km^2 (42% of Scandinavian glaciarized area), contain 61% of the total Scandinavian ice volume. In contrast, all Scandinavian glaciers with an area < 0.5 km^2 ($n = 2420$) together have an ice volume of 14.2 km^3 (4% of total volume), while they cover 393.9 km^2 (13% of total area). This small volume contained in the numerous little glaciers confirms that including the >2000 new very small glaciers (only 23 are larger than 0.1 km^2) detected recently by Andreassen and others (2022) would not have changed the overall Scandinavian ice volume appreciably. Indeed, to obtain a first-order estimate, we multiply the mean modelled thickness of all glaciers with an area smaller than 0.1 km^2 by the total area covered by the new glaciers (48 km^2) which yields an ice volume of 2.1 km^3 which we are potentially missing. Considering individual RGI60 glaciers instead of the glacier complexes, the most voluminous glacier in Sweden is Salajekna with 3.2 km^3, although it partially lies in Norway. The largest glacier by volume completely located in Sweden is the neighboring Stuorrajekna with an ice volume of 1.8 km^3. In Norway, the most voluminous glacier is Austerdalsisen (an outlet glacier of the Svartisen-Østisen ice cap) with 13.6 km^3. On that ice cap as well as on Jostedalsbreen we also find the largest ice thicknesses just above 600 m.

5.2 Bed shapes

Besides ice volume, another main result of this study is a distributed map of bed topography and ice thickness for every glacier and ice cap in Scandinavia. While all results are available from INSERT LINK TO REPOSITORY, we here show the example of an ice cap (Hardangerjøkulen) including observed thicknesses (Fig. 5) and of smaller mountain glaciers in central Norway (Fig. 6). We find that our modelled thickness field for Hardangerjøkulen is smooth but with clear variations in ice thickness, suggesting a variable subglacial topography. This agrees well with the observations, thus providing strong evidence that the obtained bed shape is realistic. Indeed, the general thickness pattern seems to be very well reproduced even where there are strong gradients in thickness, although the magnitude of certain subglacial features (e.g. the depth of a subglacial valley) may not always be matched exactly. Thanks to the approach of modelling the entire ice cap as one a bed topography free of artificial steps at the boundary of RGI60 flow units is obtained. For the central Norwegian mountain glaciers, our results likewise show an overall realistic pattern.

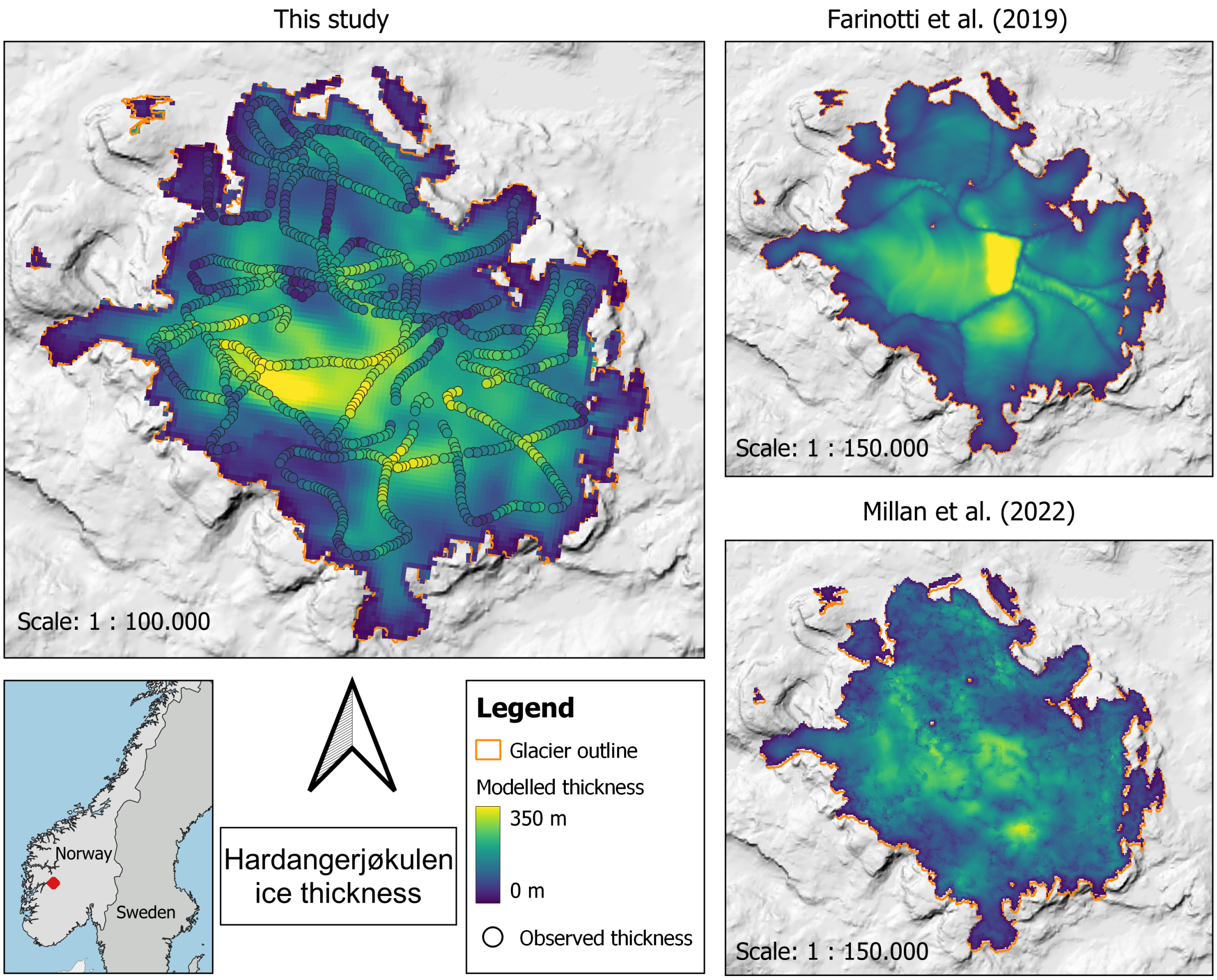

Fig. 5. Modelled ice thickness for the ice cap Hardangerjøkulen from this study as well as Farinotti and others (2019a) and Millan and others (2022). Overlain on the results of this study are observations of ice thickness from the Glacier Thicknesss Database (GlaThiDa Consortium, 2020), originally collected by Sellevold and Kloster (1964); Østen (1998); Elvehøy and others (2002).

https://doi.org/10.1017/jog.2024.25 Published online by Cambridge University Press

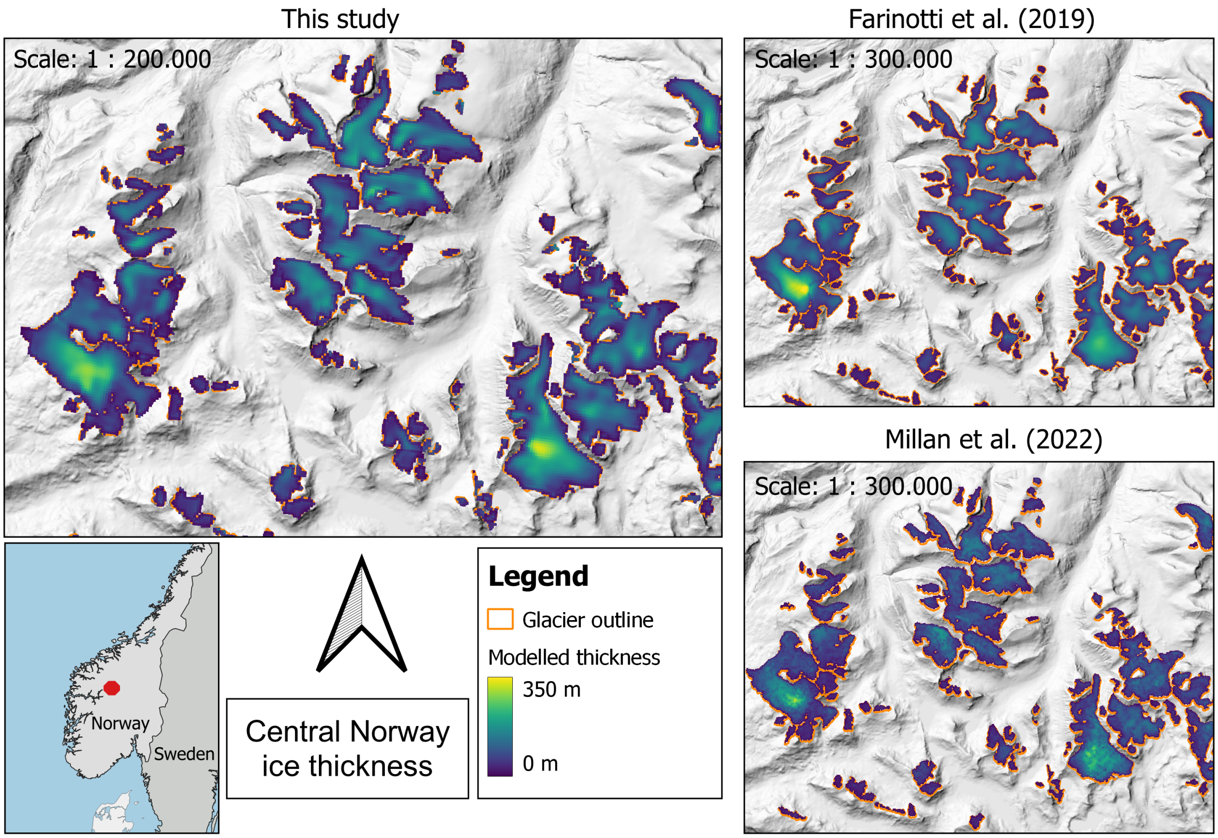

Fig. 6. Modelled ice thickness for mountain glaciers in central Norway from this study, from Farinotti and others (2019a) and from Millan and others (2022).

https://doi.org/10.1017/jog.2024.25 Published online by Cambridge University Press

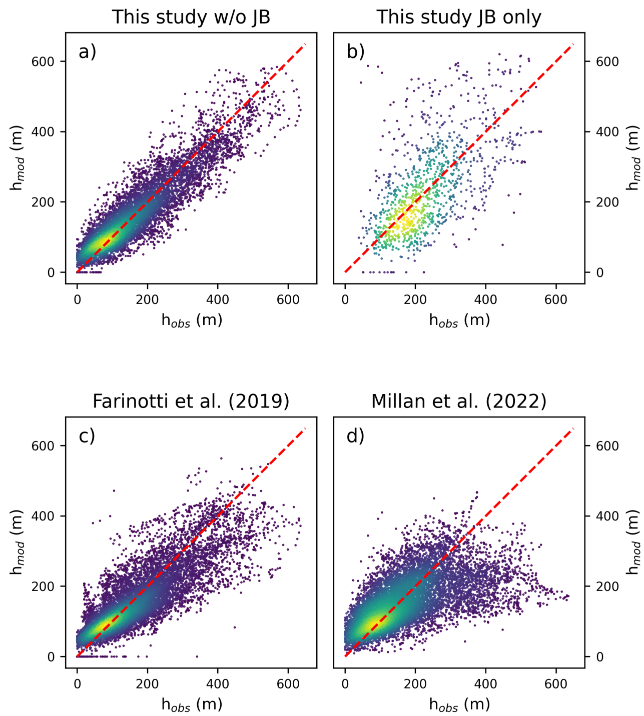

Fig. 7. Correlation between modelled and observed ice thicknesses for this study for all glaciers except Jostedalsbreen (a), for Jostedalsbreen alone (b), for Farinotti and others (2019a) (c) and for Millan and others (2022) (d) with colors indicating point density and the red dashed line denoting the diagonal.

5.3 Validation

We find a good overall agreement between modelled and observed thicknesses with errors evenly spread around zero (Fig. 7a; Table 1). With the optimized values for $A = 70\,\mathrm{MPa}^{-3}\mathrm{a}^{-1}$ and $c = 100\,\mathrm{km\,MPa}^{-3}\mathrm{a}^{-1}$, the bias to all thickness observations pooled together is 0.8 m (for comparison, the bias obtained for the upper and lower ice volume estimate is -14.8 m and 8.3 m, respectively). The mean absolute difference is 40 m, indicating that on average the modelled ice thickness at the observation locations is off by this value. Given a mean ice thickness of the observations of 165 m, this corresponds to an average thickness uncertainty of 24%. The correlation coefficient r is 0.87 demonstrating that the approach captures the Scandinavian ice thickness distribution very well, and it lends trust to the modelled bed shapes. We also compute the variance of ice thickness for all observations and the model output at those locations where there are observations; if the modelled variance is much smaller, the modelled bed is likely too smooth. For the same reason, we also consider the slope of the linear regression between h_{obs} and h_{mod}. A slope of one

https://doi.org/10.1017/jog.2024.25 Published online by Cambridge University Press

	RMSE (m)	MAD (m)	Bias (m)	slope	Pearson´s r	$\Delta\sigma^2$ (%)
This study	55	40	0.8	0.82	0.87	−12
Farinotti et al. (2019)	63	46	−9.2	0.66	0.83	−36
Milan et al. (2022)	93	66	−14.5	0.38	0.59	−57

Table 1. Descriptive statistics for thickness products from this study and previous work in relation to thickness observations. Root mean square error (RMSE), mean absolute difference (MAD), mean difference/bias, slope of the linear regression between modelled and observed thicknesses, Pearson´s correlation coefficient r and percentage difference in variance between $\mathrm{h}_{\mathrm{obs}}$ and h_{mod} at those locations where thickness observations are available ($\Delta\sigma^2$).

demonstrates that both low and high ice thicknesses are accurately captured. If the slope is significantly lower than one, as is often found for modelled ice thickness products, it usually implies that low thicknesses are over- and high ones underestimated, again due to too-smooth bed shapes. We obtain a variance that is 12% lower than the observations and a slope of 0.82 which is a good result compared to other studies (sec. 6). This, too, indicates that not only the total ice volume but also the bed shape is well captured and realistic.

We find that the largest outliers in the thickness errors are found for Jostedalsbreen, even after calibrating it separately (Fig. 7b). Indeed, comparing modelled against observed thicknesses for all other glaciers together yields a MAD of only 35 m (corresponding to an average thickness uncertainty of 22%) and a RMSE of 46 m, indicating a close clustering of points around the diagonal (Fig. 7a). The 99th percentile of absolute errors is limited to 134 m for those glaciers meaning that there is virtually no point in space outside Jostedalsbreen where the true ice thickness should be off by more than this value. Meanwhile, the MAD for Jostedalsbreen alone is 82 m (35% of ice thickness).

For further validation, we consider glaciers that have such dense radar coverage that their ice volume can be established accurately through interpolation. We compare the observed ice volume as reported in the literature with the modelled values (Table 2) and find very good agreement. All modelled volumes are close to the observations and well within their uncertainty range, with no apparent bias.

https://doi.org/10.1017/jog.2024.25 Published online by Cambridge University Press

Glacier	V_{obs} (km^3)	V_{mod} (km^3)	Reference
Blåmannsisen	14±1.7	14.0	Andreassen and others (2015)
Søndre Folgefonna	28±3.3	28.3	Ekblom Johansson and others (2022)
Nodre Folgefonna	2.7±0.5	2.7	Andreassen and others (2015)
Hardangerjøkulen	11 ± 1.4	10.6	Andreassen and others (2015)
Storglaciären	0.25	0.3	Björnsson (1981)

Table 2. Observed (V_{obs}) and modelled (V_{mod}) ice volumes for ice caps and glaciers in Scandinavia that have such dense radar coverage that their ice volume can be considered known. All values on V_{obs} are directly from the literature except for Storglaciären where the ice volume was calculated by subtracting the bed topography by Björnsson (1981) (with no published error estimate) from a current DEM.

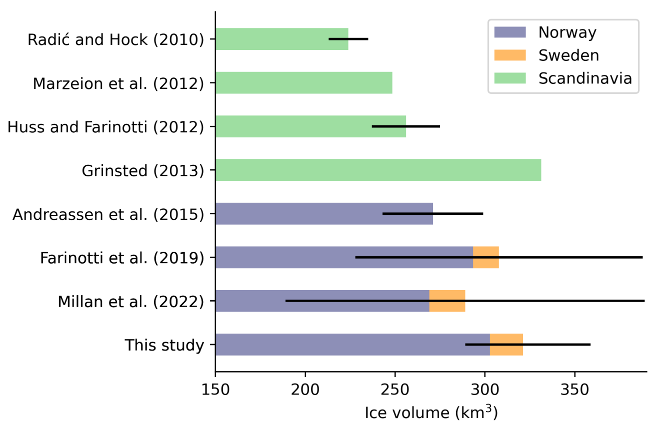

Fig. 8. Ice volume estimates from this study and previous work given either for Norway, Sweden or entire Scandinavia. Black lines indicate error estimates on the Scandinavian-wide ice volume (except for Andreassen and others (2015) where the error bar is on the Norwegian ice volume) as reported in the respective publications. Note the non-zero origin of the x-axis.

https://doi.org/10.1017/jog.2024.25 Published online by Cambridge University Press

6 DISCUSSION

6.1 Ice volume

Our calibrated ice volume estimate of 321.1 km^3 for Scandinavia with an estimated uncertainty range between 289.0 and 358.8 km^3 is generally within the limits of previously published values (Fig. 8). However, it is significantly larger than the early works by Radić and Hock (2010); Marzeion and others (2012) (which were based on volume-area scaling (Bahr and others, 1997)) and Huss and Farinotti (2012). It is also somewhat larger than what the more recent global studies by Farinotti and others (2019a); Millan and others (2022) calculated although the differences are small and well within the uncertainty bounds. The only previous study predicting a larger ice volume than this study is Grinsted (2013) with $\sim$ 330 km^3. Andreassen and others (2015) conducted a dedicated study on Norwegian ice volume combining different methods with observations and arrived at a 'best guess' of 271$\pm$28 km^3, although the total spread between methods was from 257 to 300 km^3. This, too, tends to be less than what we obtain but again, the uncertainty ranges clearly overlap with ours (272.5 to 337.5 km^3 for Norway).

The only Scandinavian thickness products that are available as distributed grids and hence allow validation against observed ice thicknesses are the ones by Farinotti and others (2019a); Millan and others (2022). Both of them show a larger negative bias than our study (Table 1) indicative of an ice volume underestimation. Meanwhile, the close match that we obtain for the glaciers with known ice volume (Table 2) may suggest that our Scandinavia-wide uncertainties are rather conservative.

6.2 Bed shape

The early studies based on volume area scaling by Radić and Hock (2010); Marzeion and others (2012); Grinsted (2013) only yielded the mean ice thickness per glacier, no bed shape. The remaining works shown in Fig. 8 produce distributed thickness fields although Huss and Farinotti (2012); Farinotti and others (2019a) completely or partially rely on flow-line approaches at heart. As shown in Table 1, the product from Farinotti and others (2019a) generally has larger errors than our results as indicated by the RMSE, MAD and r statistics. Also in terms of slope and $\Delta\sigma^2$, there are clear differences. The values obtained for our study (slope = 0.82, $\Delta\sigma^2$ = -12%) indicate that our modelled bed is smoother than reality, but given that there is a theoretical limit to how much detail in bed topography can be obtained through an ice thickness inversion (Gudmundsson, 2003; Raymond and Gudmundsson, 2005), we find the results

https://doi.org/10.1017/jog.2024.25 Published online by Cambridge University Press

satisfactory. For Farinotti and others (2019a) the slope and $\Delta\sigma^2$ are considerably lower (slope = 0.66, $\Delta\sigma^2$ = -37%) indicating that their computed bed is considerably too smooth. This is confirmed by Fig. 7c where a clear tendency towards overestimating small thicknesses and underestimating large ones can be seen. A possible explanation for that is the ensemble approach underlying the methodology in Farinotti and others (2019a) which naturally results in smoother results. The thickness product by Millan and others (2022) appears to align the least with the known ice thicknesses given the statistics in Table 1. As is also seen in Fig. 7d, the modelled thicknesses are generally less precise than those of this study and Farinotti and others (2019a), and there is a clear underestimation of large thicknesses. Given that Millan and others (2022) rely on remotely-sensed velocity observations to compute ice thicknesses, the slow flow of most Scandinavian glaciers and consequently, the weak signal obtained is a likely cause for that. These difficulties in obtaining reliable ice flow velocities are also the reason why we did not use velocity observations to calibrate ice viscosity and sliding, as was suggested as a possible strategy for mountain glaciers in Frank and others (2023). Experiments not shown here yielded consistently too-thin ice compared to observations.

Besides the statistical perspective, a visual inspection of the modelled thickness fields provides context on the quality of a thickness product. As concluded from Figs. 5 and 6, our methodology produces realistic bed shapes both for ice caps and mountain glaciers. This is not necessarily the case for the products from Farinotti and others (2019a); Millan and others (2022) (Fig. 5b,c). In the former, clear boundaries between RGI60 flow units as well as "stripes" perpendicular to the flow direction can be seen for the ice cap Hardangerjøkulen. Both of these features are related to the underlying flow-line approach which is generally known to perform poorly on ice caps (Huss and Farinotti, 2012). For mountain glaciers, however, the results from Farinotti and others (2019a) visually appear well confirming the strength of the methodology when applied to this glacier type. The results by Millan and others (2022) are somewhat noisy for both the ice cap and the mountain glaciers, again due to the methodological dependence on remotely-sensed ice flow velocities. If taken at face value, these results would imply a highly unrealistic bed topography. Also the general thickness distribution of Hardangerjøkulen is not well captured as the observed thickness maxima of around 350 m are not reproduced.

The origin of the larger errors which we obtain at Jostedalsbreen (MAD=35% of local ice thickness) compared to all other glaciers (MAD = 22%) is difficult to pinpoint. One possible explanation is that the thickness observations of Jostedalsbreen in the GlaThiDa date back to the 1980s (Kennet, 1989; GlaThiDa Consortium, 2020) with only limited documentation, making it difficult to assess data quality, potential

https://doi.org/10.1017/jog.2024.25 Published online by Cambridge University Press

biases or projection errors that could explain the large spread of the point cloud in Fig. 7b. Indeed, there are some locations where all three thickness studies available (this work, Farinotti and others (2019a), Millan and others (2022)) unanimously indicate clearly larger values than the observations. Another reason could be that the low surface slopes of such a large ice cap are generally more inducive of large thickness errors in inversion products since bed undulations leave only small surface expressions (Gudmundsson, 2003). Lastly, the topography surrounding Jostedalsbreen is generally very steep and spatially variable, suggesting that it could look similar under the ice which would naturally result in larger errors. We find that the error distribution for Jostedalsbreen is skewed with a median absolute error of 67 m (28% of local thickness), indicating that a few large outliers dominate the mean error. Therefore, if considering the median instead of the mean error, the value obtained is similar to the error that most thickness inversions yield which is typically at around 30% of the ice thickness (Farinotti and others, 2017, 2021).

6.3 Future perspectives

The methodology presented here is novel for Scandinavia in that it uses a full numerical ice dynamics model on a distributed grid to invert for ice thickness (Frank and others, 2023). Thanks to using dh/dt to infer subglacial topography, the bed shapes computed are in line with the dynamic state of the modelled glaciers, meaning that prognostic simulations of glacier evolution could be conducted without requiring any additional spin-up. Another benefit of the applied methodology is that it can readily profit from further improvements in input data quality which is not the case for approaches that are limited by the dependence on simplified ice physics. Indeed, all previous studies conducted in Scandinavia relied on volume-area scaling or simplified shallow ice physics, often applied along flow-lines, in contrast to the higher-order physics in IGM. Experiments not shown here using a SIA model instead of IGM yielded unrealistic bed shapes which can be linked directly to the insufficiently complete ice flow physics with the SIA. Specifically, ice flow with the SIA is strictly downhill (Hutter, 1983), meaning that in an inversion context local topographic minima in the glacier surface accumulate ice and become very thick. Likewise, the convex across-flow profile of glaciers as seen in the DEMs directs ice flow with the SIA to the glacier margins. When doing an inversion this leads to larger ice thicknesses on the glacier margins than in the center. While flow-line approaches are not affected by these issues in the same way, these examples underscore the value of using sophisticated ice dynamics when modelling on a distributed grid.

Nevertheless, local errors in ice thickness remain which we attribute mostly to originate from errors in modelled flow directions as it has been shown that the methodology in general is not very sensitive to either initial conditions, parameter choices or climatic mass balance and *dh*/*dt* errors (Frank and others, 2023). While these erroneous flow directions may be the result of omitting terms in the higher-order model as compared to the full-Stokes equations (Blatter, 1995; Pattyn, 2003), and hence of incomplete ice dynamics, they can also be caused by other factors related to input data or modelled processes. It has been shown that thickness inversions are highly sensitive to the input DEM as surface shape controls both flow directions and absolute thicknesses via the surface angle (Gudmundsson, 2003; Chen and others, 2022). Since we are using high-quality products from the national mapping authorities of Sweden and Norway we estimate errors associated with those to be overall small. However, even accurate DEMs do not immunize against certain topographic issues, for instance that in an inversion context, middle moraines protruding from the surrounding ice are interpreted as ice dynamical features formed by flow over a subglacial ridge, rather than as sediment lying on top of the glacier.

Further improvements in a future study could include the use of temporally more consistent input data sets which are currently not available. Due to the different time stamps of the inputs used here (Fig. 2) errors are likely introduced in the modelled thickness field, e.g. where parts of the DEM inside the RGI60 outlines show deglaciated terrain. Another difficulty arising from temporally inconsistent inputs is to establish what time our thickness product actually represents. Given that the mean year of the RGI60 outlines is 2003 (RGI Consortium, 2017), the mean of the climatic mass balance and *dh*/*dt* is 2010 (Hugonnet and others, 2021; Rounce and others, 2023) and an estimate for the mean for the DEMs is 2012, we suggest to refer to our results as representing the period 2003 - 2012. Note, however, that assigning a time stamp to a product derived from temporally mismatched inputs is rather hypothetical, and so the given period is a mere estimate. If we accept that the computed ice thickness distribution corresponds to the above mentioned period, a first estimate on the Norwegian ice loss relative to the years 2018-2019 when new glacier outlines are available for the country (Andreassen and others, 2022) can be made by considering the ice volume stored in those areas that have become ice-free over the time interval. We find that 18.5 km^2 of ice are located outside the most recent glacier outlines, i.e. 6% of the Norwegian ice volume may have disappeared over an approximate time span of 6-16 years. Note that this is only a first estimate due to the difficulties of establishing a precise time stamp of our product as specified above, and because we do not take into account neither adjustments of ice dynamic processes nor thinning in those areas that have not become ice free.

https://doi.org/10.1017/jog.2024.25 Published online by Cambridge University Press

Lastly, more thickness observations would be of great help to improve future ice thickness inversions in Scandinavia. Currently, there is an over-representation of large ice caps among the ice bodies with observations (GlaThiDa Consortium, 2020). Since the ice caps are un-proportionally voluminous compared to the many smaller mountain glaciers (sec. 5), this is not necessarily disadvantageous. However, more observations on smaller glaciers would allow for a better calibration there and could reduce the uncertainty on ice volume further. This is particularly true for Swedish glaciers where publicly available thickness observations are lacking almost entirely, meaning that the calibration for these glaciers is currently reliant on Norwegian observations obtained in a different climatic setting.

7 CONCLUSIONS

We here produced a new map of distributed bed topography and ice thickness alongside an updated ice volume estimate for each glacier and ice cap in Scandinavia. We anticipate that this product will be of benefit in a variety of applications, such as for water management in the context of hydropower production, for risk assessment of glacier lake outburst floods and landslides, for the planning of scientific projects, for the tourism industry and for future projections of glacier response to climate warming. The calibrated ice volume estimate for Scandinavia of 321.1 km^3 with an uncertainty range of 289.0 km^3 and 358.8 km^3 is similar to, although slightly larger than, recent estimates proposed. Thanks to the novel methodology, this study is the first to provide realistic bed maps for all glaciers and ice caps in Scandinavia, outperforming previous studies (Farinotti and others, 2019a; Millan and others, 2022) as shown by validation against thickness observations. Nevertheless, we find that the global perspective of the studies by Farinotti and others (2019a) and Millan and others (2022) and their methodologically simpler approaches as compared to this work have not resulted in in-accurate ice volume estimates for Scandinavia. However, when it comes to the computed bed shapes the product by Farinotti and others (2019a) suffers from clear issues on ice caps while the results by Millan and others (2022) are adversely affected by challenges in mapping the flow speeds of slow glaciers. We deem it likely that similar issues in these products are present in other regions on Earth, suggesting that future studies could seek to provide a further improved global ice thickness product.

https://doi.org/10.1017/jog.2024.25 Published online by Cambridge University Press

8 ACKNOWLEDGEMENTS

We thank David Rounce for kindly sharing climatic mass balance data with us. This research has been supported by Vetenskapsrådet (grant no. 2020-04319) and Rymdstyrelsen (189/18). The computations were enabled by resources provided by the National Academic Infrastructure for Supercomputing in Sweden (NAISS) at Chalmers partially funded by the Swedish Research Council through grant agreement no. 2022-06725.

9 DATA AVAILABILITY

Upon acceptance of the paper, ice thickness and bed topography maps will be made publicly available as GeoTiffs through a data repository.

REFERENCES

Andreassen LM (2022) Breer og fonner i Norge. Technical Report 3–2022, Norwegian Water Resources and Energy Directorate, Oslo, Norway

Andreassen LM, Winsvold (eds) S, Paul F and Hausberg J (2012) *Inventory of Norwegian Glaciers*. Number 28-2012 in NVE Rapport, Norwegian Water Resources and Energy Directorate, Oslo, Norway, ISBN 978-82-410-0826-9

Andreassen LM, Huss M, Melvold K, Elvehøy H and Winsvold SH (2015) Ice thickness measurements and volume estimates for glaciers in Norway. *Journal of Glaciology*, **61**(228), 763–775, ISSN 0022-1430, 1727-5652 (doi: 10.3189/2015JoG14J161)

Andreassen LM, Elvehøy H, Kjøllmoen B and Belart JMC (2020) Glacier change in Norway since the 1960s – an overview of mass balance, area, length and surface elevation changes. *Journal of Glaciology*, **66**(256), 313–328, ISSN 0022-1430, 1727-5652 (doi: 10.1017/jog.2020.10)

Andreassen LM, Nagy T, Kjøllmoen B and Leigh JR (2022) An inventory of Norway's glaciers and ice-marginal lakes from 2018–19 Sentinel-2 data. *Journal of Glaciology*, **68**(272), 1085–1106, ISSN 0022-1430, 1727-5652 (doi: 10.1017/jog.2022.20)

Bahr DB, Meier MF and Peckham SD (1997) The physical basis of glacier volume-area scaling. *Journal of Geophysical Research: Solid Earth*, **102**(B9), 20355–20362, ISSN 2156-2202 (doi: 10.1029/97JB01696)

Bahr DB, Pfeffer WT and Kaser G (2014) Glacier volume estimation as an ill-posed inversion. *Journal of Glaciology*, **60**(223), 922–934, ISSN 0022-1430, 1727-5652 (doi: 10.3189/2014JoG14J062)

Björnsson H (1981) Radio-Echo Sounding Maps of Storglaciären, Isfallsglaciären and Rabots Glaciär, Northern Sweden. *Geografiska Annaler: Series A, Physical Geography*, **63**(3-4), 225–231, ISSN 0435-3676 (doi: 10.1080/04353676.1981.11880037)

Blatter H (1995) Velocity and stress fields in grounded glaciers: a simple algorithm for including deviatoric stress gradients. *Journal of Glaciology*, **41**(138), 333–344, ISSN 0022-1430, 1727-5652 (doi: 10.3189/S002214300001621X)

Bosson JB, Huss M, Cauvy-Fraunié S, Clément JC, Costes G, Fischer M, Poulenard J and Arthaud F (2023) Future emergence of new ecosystems caused by glacial retreat. *Nature*, **620**(7974), 562–569, ISSN 1476-4687 (doi: 10.1038/s41586-023-06302-2)

Breien H, De Blasio FV, Elverhøi A and Høeg K (2008) Erosion and morphology of a debris flow caused by a glacial lake outburst flood, Western Norway. *Landslides*, **5**(3), 271–280, ISSN 1612-5118 (doi: 10.1007/s10346-008-0118-3)

Chen W, Yao T, Zhang G, Li F, Zheng G, Zhou Y and Xu F (2022) Towards ice-thickness inversion: an evaluation of global digital elevation models (DEMs) in the glacierized Tibetan Plateau. *The Cryosphere*, **16**(1), 197–218, ISSN 1994-0416 (doi: 10.5194/tc-16-197-2022)

Cuffey KM and Paterson WSB (2010) *The physics of glaciers*. Butterworth-Heinemann, Amsterdam, ISBN 978-0-12-369461-4

Ekblom Johansson F, Bakke J, Støren EN, Gillespie MK and Laumann T (2022) Mapping of the Subglacial Topography of Folgefonna Ice Cap in Western Norway—Consequences for Ice Retreat Patterns and Hydrological Changes. *Frontiers in Earth Science*, **10**, ISSN 2296-6463

Elvehøy H, Engeset RV, Andreassen LM, Kohler J, Gjessing Y and Björnsson H (2002) Assessment of possible jökulhlaups from Lake Demmevatn in Norway. *IAHS-AISH publication*, 31–36

Engeset RV, Schuler TV and Jackson M (2005) Analysis of the first jökulhlaup at Blåmannsisen, northern Norway, and implications for future events. *Annals of Glaciology*, **42**, 35–41, ISSN 0260-3055, 1727-5644 (doi: 10.3189/172756405781812600)

Farinotti D, Huss M, Bauder A, Funk M and Truffer M (2009) A method to estimate the ice volume and ice-thickness distribution of alpine glaciers. *Journal of Glaciology*, **55**(191), 422–430, ISSN 0022-1430, 1727-5652 (doi: 10.3189/002214309788816759)

Farinotti D, Brinkerhoff DJ, Clarke GKC, Fürst JJ, Frey H, Gantayat P, Gillet-Chaulet F, Girard C, Huss M, Leclercq PW, Linsbauer A, Machguth H, Martin C, Maussion F, Morlighem M, Mosbeux C, Pandit A, Portmann A, Rabatel A, Ramsankaran R, Reerink TJ, Sanchez O, Stentoft PA, Singh Kumari S, van Pelt WJJ, Anderson B, Benham T, Binder D, Dowdeswell JA, Fischer A, Helfricht K, Kutuzov S, Lavrentiev I, McNabb R, Gudmundsson

GH, Li H and Andreassen LM (2017) How accurate are estimates of glacier ice thickness? Results from ITMIX, the Ice Thickness Models Intercomparison eXperiment. *The Cryosphere*, **11**(2), 949–970, ISSN 1994-0416 (doi: 10.5194/tc-11-949-2017)

Farinotti D, Huss M, Fürst JJ, Landmann J, Machguth H, Maussion F and Pandit A (2019a) A consensus estimate for the ice thickness distribution of all glaciers on Earth. *Nature Geoscience*, **12**(3), 168–173, ISSN 1752-0908 (doi: 10.1038/s41561-019-0300-3)

Farinotti D, Round V, Huss M, Compagno L and Zekollari H (2019b) Large hydropower and water-storage potential in future glacier-free basins. *Nature*, **575**(7782), 341–344, ISSN 1476-4687 (doi: 10.1038/s41586-019-1740-z)

Farinotti D, Brinkerhoff DJ, Fürst JJ, Gantayat P, Gillet-Chaulet F, Huss M, Leclercq PW, Maurer H, Morlighem M, Pandit A, Rabatel A, Ramsankaran R, Reerink TJ, Robo E, Rouges E, Tamre E, van Pelt WJJ, Werder MA, Azam MF, Li H and Andreassen LM (2021) Results from the Ice Thickness Models Intercomparison eXperiment Phase 2 (ITMIX2). *Frontiers in Earth Science*, **8**, ISSN 2296-6463 (doi: 10.3389/feart.2020.571923)

Fountain AG, Jacobel RW, Schlichting R and Jansson P (2005) Fractures as the main pathways of water flow in temperate glaciers. *Nature*, **433**(7026), 618–621, ISSN 1476-4687 (doi: 10.1038/nature03296)

Frank T, Åkesson H, de Fleurian B, Morlighem M and Nisancioglu KH (2022) Geometric controls of tidewater glacier dynamics. *The Cryosphere*, **16**(2), 581–601, ISSN 1994-0416 (doi: 10.5194/tc-16-581-2022)

Frank T, van Pelt WJJ and Kohler J (2023) Reconciling ice dynamics and bed topography with a versatile and fast ice thickness inversion. *The Cryosphere*, **17**(9), 4021–4045, ISSN 1994-0416 (doi: 10.5194/tc-17-4021-2023)

Frey H, Machguth H, Huss M, Huggel C, Bajracharya S, Bolch T, Kulkarni A, Linsbauer A, Salzmann N and Stoffel M (2014) Estimating the volume of glaciers in the Himalayan-Karakoram region using different methods. *The Cryosphere*, **8**(6), 2313–2333, ISSN 1994-0416 (doi: 10.5194/tc-8-2313-2014)

Gantayat P, Kulkarni AV and Srinivasan J (2014) Estimation of ice thickness using surface velocities and slope: case study at Gangotri Glacier, India. *Journal of Glaciology*, **60**(220), 277–282, ISSN 0022-1430, 1727-5652 (doi: 10.3189/2014JoG13J078)

GlaThiDa Consortium (2020) Glacier Thickness Database 3.1.0

Grinsted A (2013) An estimate of global glacier volume. *The Cryosphere*, **7**(1), 141–151, ISSN 1994-0416 (doi: 10.5194/tc-7-141-2013)

Grove JM (2004) *The Little Ice Age*. Routledge, London, 2 edition, ISBN 978-0-203-50520-5 (doi: 10.4324/9780203505205)

Gudmundsson GH (2003) Transmission of basal variability to a glacier surface. *Journal of Geophysical Research: Solid Earth*, **108**(B5), ISSN 2156-2202 (doi: 10.1029/2002JB002107)

Habermann M, Maxwell D and Truffer M (2012) Reconstruction of basal properties in ice sheets using iterative inverse methods. *Journal of Glaciology*, **58**(210), 795–808, ISSN 0022-1430, 1727-5652 (doi: 10.3189/2012JoG11J168)

Haeberli W and Hoelzle M (1995) Application of inventory data for estimating characteristics of and regional climate-change effects on mountain glaciers: a pilot study with the European Alps. *Annals of Glaciology*, **21**, 206–212, ISSN 0260-3055, 1727-5644 (doi: 10.3189/S0260305500015834)

Hock R and Holmgren B (2005) A distributed surface energy-balance model for complex topography and its application to Storglaciären, Sweden. *Journal of Glaciology*, **51**(172), 25–36

Holmlund P and Eriksson M (1989) The Cold Surface Layer on Storglaciären. *Geografiska Annaler: Series A, Physical Geography*, **71**(3-4), 241–244, ISSN 0435-3676, 1468-0459 (doi: 10.1080/04353676.1989.11880291)

Holmlund P and Jansson P (1999) The Tarfala Mass Balance Programme. *Geografiska Annaler, Series A: Physical Geography*, **81**(4), 621–631, ISSN 0435-3676, 1468-0459 (doi: 10.1111/j.0435-3676.1999.00090.x)

Holmlund P, Karlén W and Grudd H (1996) Fifty Years of Mass Balance and Glacier Front Observations at the Tarfala Research Station. *Geografiska Annaler: Series A, Physical Geography*, **78**(2-3), 105–114, ISSN 0435-3676, 1468-0459 (doi: 10.1080/04353676.1996.11880456)

Hooke RL, Calla P, Holmlund P, Nilsson M and Stroeven A (1989) A 3 year record of seasonal variations in surface velocity, Storglaciären, Sweden. *Journal of Glaciology*, **35**(120), 235–247

Hugonnet R, McNabb R, Berthier E, Menounos B, Nuth C, Girod L, Farinotti D, Huss M, Dussaillant I, Brun F and Kääb A (2021) Accelerated global glacier mass loss in the early twenty-first century. *Nature*, **592**(7856), 726–731, ISSN 1476-4687 (doi: 10.1038/s41586-021-03436-z)

Huss M (2013) Density assumptions for converting geodetic glacier volume change to mass change. *The Cryosphere*, **7**(3), 877–887

Huss M and Farinotti D (2012) Distributed ice thickness and volume of all glaciers around the globe. *Journal of Geophysical Research: Earth Surface*, **117**(F4), ISSN 2156-2202 (doi: 10.1029/2012JF002523)

Hutter K (1983) *Theoretical glaciology: materials science of ice and the mechanics of glaciers and ice sheets*. Mathematical approaches to geophysics, Reidel, Dordrecht, ISBN 978-90-277-1473-2

Jackson M and Ragulina G (2014) Inventory of glacier-related hazardous events in Norway. *Norges vassdrags-og energidirektorat (NVE)/Norwegian Water Resources and Energy Directorate, Report*, **83**, 213

Jouvet G (2022) Inversion of a Stokes glacier flow model emulated by deep learning. *Journal of Glaciology*, 1–14, ISSN 0022-1430, 1727-5652 (doi: 10.1017/jog.2022.41)

Jouvet G and Cordonnier G (2023) Ice-flow model emulator based on physics-informed deep learning. *Journal of Glaciology*, 1–15, ISSN 0022-1430, 1727-5652 (doi: 10.1017/jog.2023.73)

Jouvet G, Cordonnier G, Kim B, Lüthi M, Vieli A and Aschwanden A (2022) Deep learning speeds up ice flow modelling by several orders of magnitude. *Journal of Glaciology*, **68**(270), 651–664, ISSN 0022-1430, 1727-5652 (doi: 10.1017/jog.2021.120)

Karlén W (1973) Holocene Glacier and Climatic Variations, Kebnekaise Mountains, Swedish Lapland. *Geografiska Annaler: Series A, Physical Geography*, **55**(1), 29–63, ISSN 0435-3676 (doi: 10.1080/04353676.1973.11879879), publisher: Taylor & Francis _eprint: https://doi.org/10.1080/04353676.1973.11879879

Karlén W and Matthews JA (1992) Reconstructing Holocene Glacier Variations from Glacial Lake Sediments: Studies from Nordvestlandet and Jostedalsbreen-Jotunheimen, Southern Norway. *Geografiska Annaler: Series A, Physical Geography*, **74**(4), 327–348, ISSN 0435-3676 (doi: 10.1080/04353676.1992.11880374)

Kartverket (2013) Height DTM 50 m

Kennet M (1989) Feltavgrensning på nordre Jostedalsbreen. Technical Report 2-89, Norwegian Water Resources and Energy Directorate, Oslo, Norway

Lantmäteriet (2022) Markhöjdmodell Nedladdning, grid 50+

Liestøl O (1956) Glacier Dammed Lakes in Norway. *Norsk Geografisk Tidsskrift - Norwegian Journal of Geography*, **15**(3-4), 122–149, ISSN 0029-1951 (doi: 10.1080/00291955608542772)

Linsbauer A, Paul F, Hoelzle M, Frey H and Haeberli W (2009) The Swiss Alps without glaciers – a GIS-based modelling approach for reconstruction of glacier beds. *Proceedings of Geomorphometry*, 243–247 (doi: 10.5167/uzh-27834)

Marr P, Winkler S and Löffler J (2022) Environmental and Socio-Economic Consequences of Recent Mountain Glacier Fluctuations in Norway. In U Schickhoff, R Singh and S Mal (eds.), *Mountain Landscapes in Transition : Effects of Land Use and Climate Change*, Sustainable Development Goals Series, 289–314, Springer International Publishing, Cham, ISBN 978-3-030-70238-0 (doi: 10.1007/978-3-030-70238-$0_1$0)

Marzeion B, Jarosch AH and Hofer M (2012) Past and future sea-level change from the surface mass balance of glaciers. *The Cryosphere*, **6**(6), 1295–1322, ISSN 1994-0416 (doi: 10.5194/tc-6-1295-2012)

Millan R, Mouginot J, Rabatel A and Morlighem M (2022) Ice velocity and thickness of the world's glaciers. *Nature Geoscience*, **15**(2), 124–129, ISSN 1752-0908 (doi: 10.1038/s41561-021-00885-z)

Nye JF (1952) A Method of Calculating the Thicknesses of the Ice-Sheets. *Nature*, **169**(4300), 529–530, ISSN 1476-4687 (doi: 10.1038/169529a0)

Oppenheimer M, Glavovic B, Hinkel J, van de Wal R, Magnan A, Abd-Elgawad A, Cai R, Cifuentes-Jara M, DeConto R, Ghosh T, Hay J, Isla F, Marzeion B and Sebesvari Z (2019) Sea Level Rise and Implications for Low-Lying Islands, Coasts and Communities. In *IPCC Special Report on the Ocean and Cryosphere in a Changing Climate*

Pattyn F (2003) A new three-dimensional higher-order thermomechanical ice sheet model: Basic sensitivity, ice stream development, and ice flow across subglacial lakes. *Journal of Geophysical Research: Solid Earth*, **108**(B8), ISSN 2156-2202 (doi: 10.1029/2002JB002329)

Paul F, Winsvold SH, Kääb A, Nagler T and Schwaizer G (2016) Glacier Remote Sensing Using Sentinel-2. Part II: Mapping Glacier Extents and Surface Facies, and Comparison to Landsat 8. *Remote Sensing*, **8**(7), 575, ISSN 2072-4292 (doi: 10.3390/rs8070575)

Pettersson R, Jansson P and Holmlund P (2003) Cold surface layer thinning on Storglaciären, Sweden, observed by repeated ground penetrating radar surveys. *Journal of Geophysical Research: Earth Surface*, **108**(F1), ISSN 2156-2202 (doi: 10.1029/2003JF000024)

Pohjola VA (1993) TV-video observations of bed and basal sliding on Storglaciären, Sweden. *Journal of Glaciology*, **39**(131), 111–118, ISSN 0022-1430, 1727-5652 (doi: 10.3189/S0022143000015768)

Pritchard HD (2019) Asia's shrinking glaciers protect large populations from drought stress. *Nature*, **569**(7758), 649–654

Radić V and Hock R (2010) Regional and global volumes of glaciers derived from statistical upscaling of glacier inventory data. *Journal of Geophysical Research: Earth Surface*, **115**(F1), ISSN 2156-2202 (doi: https://doi.org/10.1029/2009JF001373)

Raup B, Kääb A, Kargel JS, Bishop MP, Hamilton G, Lee E, Paul F, Rau F, Soltesz D, Khalsa SJS, Beedle M and Helm C (2007) Remote sensing and GIS technology in the Global Land Ice Measurements from Space (GLIMS) Project. *Computers & Geosciences*, **33**(1), 104–125 (doi: 10.1016/j.cageo.2006.05.015)

Raymond MJ and Gudmundsson GH (2005) On the relationship between surface and basal properties on glaciers, ice sheets, and ice streams. *Journal of Geophysical Research: Solid Earth*, **110**(B8), ISSN 2156-2202 (doi: 10.1029/2005JB003681)

RGI Consortium (2017) *Randolph Glacier Inventory – A Dataset of Global Glacier Outlines: Version 6.0.* NSIDC: National Snow and Ice Data Center, Boulder, Colorado USA

Rounce DR, Hock R, Maussion F, Hugonnet R, Kochtitzky W, Huss M, Berthier E, Brinkerhoff D, Compagno L, Copland L, Farinotti D, Menounos B and McNabb RW (2023) Global glacier change in the 21st century: Every increase in temperature matters. *Science*, **379**(6627), 78–83 (doi: 10.1126/science.abo1324)

Sellevold M and Kloster K (1964) Seismic measurements on the glacier Hardangerjøkulen, Western Norwa. In *Norsk Polarinslitutt Årbok*, 87–91, Norsk Polarinstitutt, Oslo, Norway

Stroeven AP, Hättestrand C, Kleman J, Heyman J, Fabel D, Fredin O, Goodfellow BW, Harbor JM, Jansen JD and Olsen L (2016) Deglaciation of Fennoscandia. *Quaternary Science Reviews*, **147**, 91–121

Terleth Y, Pelt WJJv and Pettersson R (2023) Spatial variability in winter mass balance on Storglaciären modelled with a terrain-based approach. *Journal of Glaciology*, **69**(276), 749–761, ISSN 0022-1430, 1727-5652 (doi: 10.1017/jog.2022.96)

van Pelt WJJ, Oerlemans J, Reijmer CH, Pettersson R, Pohjola VA, Isaksson E and Divine D (2013) An iterative inverse method to estimate basal topography and initialize ice flow models. *The Cryosphere*, **7**(3), 987–1006, ISSN 1994-0416 (doi: 10.5194/tc-7-987-2013)

Weertman J (1957) On the sliding of glaciers. *Journal of glaciology*, **3**(21), 33–38

Welty E, Zemp M, Navarro F, Huss M, Fürst JJ, Gärtner-Roer I, Landmann J, Machguth H, Naegeli K, Andreassen LM, Farinotti D, Li H and GlaThiDa Contributors (2020) Worldwide version-controlled database of glacier thickness observations. *Earth System Science Data*, **12**(4), 3039–3055, ISSN 1866-3508 (doi: 10.5194/essd-12-3039-2020)

WGMS (2022) Fluctuations of Glaciers Database (doi: 10.5904/wgms-fog-2022-09)

Åkesson H, Nisancioglu KH and Nick FM (2018) Impact of Fjord Geometry on Grounding Line Stability. *Frontiers in Earth Science*, **6**, ISSN 2296-6463 (doi: 10.3389/feart.2018.00071)

Østen K (1998) *Radio-ekko undersøkelser på Midtdalsbreen, Sør-Norge*. Master's thesis, Department of Geography, University of Oslo, Oslo, Norway

A APPENDIX

https://doi.org/10.1017/jog.2024.25 Published online by Cambridge University Press